8-11-2014

Dynamics of methane ebullition from a peat monolith revealed from a dynamic flux chamber system

Zhongjie Yu
Rutgers University

Lee D. Slater
Rutgers University

Karina V. R. Schafer
Rutgers University

Andrew S. Reeve
University of Maine, Orono

Ruth K. Varner
University of New Hampshire, Durham, ruth.varner@unh.edu

Recommended Citation
Yu, Zhongjie, L.D. Slater, K.V.R. Schäfer, A.S. Reeve, and R.K. Varner, (2014) Dynamics of methane ebullition from a peat monolith revealed from a dynamic flux chamber system, J. Geophys. Res. Biogeosciences, 119(9): 1789–1806, doi: 10.1002/2014JG002654.

AGU PUBLICATIONS

JGR

Journal of Geophysical Research: Biogeosciences

RESEARCH ARTICLE
10.1002/2014JG002654

Key Points:
- DFC is a suitable technique for continuous measurement of CH_4 ebullition
- Multiple ebullition thresholds exist in peat regulating gas bubble dynamics
- Drops in atmospheric pressure trigger CH_4 ebullition

Supporting Information:
- Readme
- Text S1–S2, Tables S1–S3, and Figures S1–S12

Correspondence to:
Z. Yu,
zjyu1986@gmail.com

Citation:
Yu, Z., L. D. Slater, K. V. R. Schäfer, A. S. Reeve, and R. K. Varner (2014), Dynamics of methane ebullition from a peat monolith revealed from a dynamic flux chamber system, *J. Geophys. Res. Biogeosci.*, *119*, 1789–1806, doi:10.1002/2014JG002654.

Received 21 FEB 2014
Accepted 4 AUG 2014
Accepted article online 11 AUG 2014
Published online 4 SEP 2014

Dynamics of methane ebullition from a peat monolith revealed from a dynamic flux chamber system

Zhongjie Yu[1,2], Lee D. Slater[1], Karina V. R. Schäfer[3], Andrew S. Reeve[4], and Ruth K. Varner[5]

[1]Department of Earth and Environmental Sciences, Rutgers University, Newark, New Jersey, USA, [2]Now at Department of Geology and Planetary Science, University of Pittsburgh, Pittsburgh, Pennsylvania, USA, [3]Department of Biological Sciences, Rutgers University, Newark, New Jersey, USA, [4]School of Earth and Climate Sciences, University of Maine, Orono, Maine, USA, [5]Institute for the Study of Earth, Oceans, and Space and Department of Earth Sciences, University of New Hampshire, Durham, New Hampshire, USA

Abstract Methane (CH_4) ebullition in northern peatlands is poorly quantified in part due to its high spatiotemporal variability. In this study, a dynamic flux chamber (DFC) system was used to continuously measure CH_4 fluxes from a monolith of near-surface *Sphagnum* peat at the laboratory scale to understand the complex behavior of CH_4 ebullition. Coincident transmission ground penetrating radar measurements of gas content were also acquired at three depths within the monolith. A graphical method was developed to separate diffusion, steady ebullition, and episodic ebullition fluxes from the total CH_4 flux recorded and to identify the timing and CH_4 content of individual ebullition events. The results show that the application of the DFC had minimal disturbance on air-peat CH_4 exchange and estimated ebullition fluxes were not sensitive to the uncertainties associated with the graphical model. Steady and episodic ebullition fluxes were estimated to be averagely 36 ± 24% and 38 ± 24% of the total fluxes over the study period, respectively. The coupling between episodic CH_4 ebullition and gas content within the three layers supports the existence of a threshold gas content regulating CH_4 ebullition. However, the threshold at which active ebullition commenced varied between peat layers with a larger threshold (0.14 $m^3\ m^{-3}$) observed in the deeper layers, suggesting that the peat physical structure controls gas bubble dynamics in peat. Temperature variation (23°C to 27°C) was likely only responsible for small episodic ebullition events from the upper peat layer, while large ebullition events from the deeper layers were most likely triggered by drops in atmospheric pressure.

1. Introduction

Northern peatlands are a global methane (CH_4) source, accounting for about 12% of global CH_4 emissions to the atmosphere, and a net sink for atmospheric carbon dioxide (CO_2) [*Wuebbles and Hayhoe*, 2002]. Carbon cycling in these ecosystems is controlled by the interactions among microbiological, hydrogeological, plant ecological, and climatological processes [*Slater and Reeve*, 2002; *Turetsky et al*., 2008; *Bragazza et al*., 2012], which all have the potential to affect CH_4 production, oxidation, and transport dynamics [*Bridgham et al*., 2013]. During the last two decades there has been a growing interest in biogenic gas bubbles in northern peatlands. The presence of these bubbles in peat below the water table impacts the buoyancy of floating peat [*Fechner-Levy and Hemond*, 1996], results in the development of overpressured stratum [*Rosenberry et al*., 2003], decreases hydraulic conductivity and substrate delivery [*Kellner et al*., 2005], and contributes to CH_4 release from peatlands via rapid bubbling (ebullition) [*Glaser et al*., 2004]. Compared to other CH_4 transport pathways in peatlands, i.e., diffusion of dissolved CH_4 and venting of CH_4 through aerenchyma of plants, ebullition of CH_4-containing bubbles from the subsurface might release larger amounts of CH_4 and exhibit much greater spatiotemporal variation [*Christensen et al*., 2003]. Table 1 is a compilation of recent findings on CH_4 ebullition in peatlands obtained from various methods, showing that estimated ebullition fluxes vary over 4 orders of magnitude even under laboratory conditions.

Theoretically, a bubble is formed in a fully saturated peat when the total pressure of the water-dissolved gases exceeds the sum of hydrostatic pressure imposed by the water table and atmospheric pressure [*Strack et al*., 2005]. Once formed in peat, biogenic bubbles can be trapped under confining layers that consist of peat with pore diameters small enough to block the passage of bubbles [*Rosenberry et al*., 2003; *Glaser et al*., 2004].

Table 1. Gas Content, Dissolved CH_4, and Ebullition Flux in Peatlands

Gas Content	Dissolved CH_4 (mg CH_4 L^{-1})	Ebullition Flux (mg CH_4 m^{-2} d^{-1})	Method[a]	Controls on Ebullition Flux[b]	Reference
0.01–0.15	0.1–11.7	2–83	Gas trap (L)	Bubble threshold	*Baird et al.* [2004]
		0–196	DFC (L)	AT	*Beckmann et al.* [2004]
		45–225	DFC (L)	Surface vegetation	*Christensen et al.* [2004]
		3–68	Gas trap with time-lapse camera (F)	AP	*Comas and Wright* [2012]
	0.1–1.3[c]	0.2–784	CSC (L)	Surface vegetation	*Green and Baird* [2012]
	1.9–6.0	<10	CSC (L)	AP	*Green and Baird* [2013]
		49–152[d]	Automated CSC (F)	CH_4 production, wind speed, water table	*Goodrich et al.* [2011]
0.02–0.16	11.7–13.9	270	Gas trap (L)	Bubble threshold, AP, AT	*Kellner et al.* [2006]
		7–12	Gas trap (F)	None	*Stamp et al.* [2013]
0.05–0.15[e]	0.1–5.8	65	Gas trap (F)	AP, water table	*Strack et al.* [2005]
	~ 10.5[f]	76–1233	CSC (L)	AP	*Tokida et al.* [2005]
		48–1440	CSC (F)	AP	*Tokida et al.* [2007]
0.03–0.15	1.0–11.6	1471–33093	Gas trap (L)	AP, AT	*Waddington et al.* [2009]
0.04–0.15	0.1–11.2	0–237	DFC (L)	AP, AT	This study

[a]Methods for ebullition flux measurement. L and F in the brackets denote laboratory study and field study, respectively.
[b]AP and AT denote atmospheric pressure and atmospheric temperature, respectively.
[c]Estimated from Figure 4 in the original paper.
[d]Flux was obtained by multiplying seasonally averaged ebullition event flux to mean CH_4 concentration for each event.
[e]Change in volumetric gas content relative to the beginning point.
[f]Depth-averaged value, estimated by assuming partial pressure representing 45% by volume of CH_4 in bubbles.

Bubbles migrate upward to the water table once buoyancy forces surpass the trapping forces at the bubble-peat interface [*Kellner et al.*, 2005]. One potential reason for the high spatiotemporal variability and the episodic nature of CH_4 ebullition is that a large bubble-storage capacity of peat may result in a partial decoupling between biological CH_4 production and bubble dynamics in subsurface peat [*Strack and Waddington*, 2008], such that physical factors can determine and/or alter the mechanical balance of the bubble-peat interaction, triggering CH_4 ebullition [*Tokida et al.*, 2009]. Results from laboratory incubations of poorly decomposed near-surface *Sphagnum* peat (*S. papillosum* and *S. magellanicum*) suggest that there is a threshold gas content of 10–16% by volume, depending on the effective compressibility of peat, that must be reached in the peat matrix before the main period of ebullition [*Baird et al.*, 2004; *Kellner et al.*, 2006]. Changes in environmental factors, particularly atmospheric pressure and temperature (Table 1), may trigger ebullition through their direct impact on bubble volume as described by the Ideal Gas Law and Henry's Law [*Tokida et al.*, 2009]. Indeed, CH_4 ebullition in northern peatlands can often be treated as a net consequence of mechanical disequilibrium associated with coupled belowground and aboveground hydroclimatological changes [*Fechner-Levy and Hemond*, 1996].

Closed static chambers (CSCs) and gas traps have been widely used to quantify ebullition fluxes in peatlands [e.g., *Tokida et al.*, 2005; *Stamp et al.*, 2013]. However, CSCs suffer from low temporal resolution, while gas traps only provide cumulative bubble volume trapped and thus an indirect ebullition flux measurement [*Mastepanov and Christensen*, 2009]. In addition, neither of these two methods is able to clarify how individual ebullition events result from triggering factors over a longer time scale. The large uncertainties associated with CH_4 ebullition estimates may, in part, result from a lack of suitable monitoring methods [*Christensen et al.*, 2003; *Mastepanov and Christensen*, 2009]. More recently, *Goodrich et al.* [2011] observed a prominent diel variation of CH_4 ebullition in a temperate peatland over three seasons using automatic flux chambers with a high sampling frequency. This study highlights the need for continuous flux measurements in order to obtain accurate ebullition estimates. Furthermore, although an ebullition threshold may be used to reasonably predict bubble release by volume in the laboratory [*Kellner et al.*, 2006], it provides little insight into how physical characteristics of peat control the relationship between bubble entrapment and ebullition fluxes [*Coulthard et al.*, 2009]. The integration of continuous flux measurement and subsurface bubble monitoring is thus required to gain a better process-based understanding of the complex behavior of CH_4 ebullition.

As a step toward better understanding of the importance of CH_4 ebullition fluxes, we developed a dynamic flux chamber (DFC) for the continuous monitoring of CH_4 ebullition from a near-surface peat monolith under

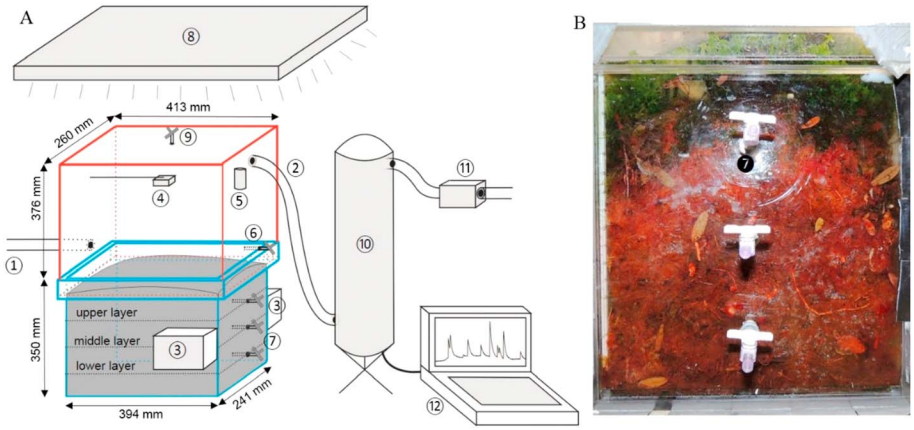

Figure 1. (a) Schematic of dynamic flux chamber system consisting of the following: (1) inflowing duct, (2) outflowing duct, (3) 1.2 GHz GPR antennae, (4) mixing fan, (5) RHT 50 environmental sensor, (6) standpipe for regulating water table, (7) pore water sampling ports, (8) florescent light, (9) gas sampling port, (10) LI-7700 fast methane analyzer, (11) vacuum pump with a vacuum regulator, and (12) computer; (b) side view showing stratum characteristics for the three layers.

laboratory conditions. A fast methane analyzer (FMA) providing high-precision CH_4 concentration measurements at 5 Hz was incorporated into the system for the quantification of both steady state and ebullitive CH_4 fluxes. Ground penetrating radar (GPR), a noninvasive geophysical method, was used to estimate gas content in peat [*Comas and Slater*, 2007] in conjunction with the measurement of dissolved CH_4 concentrations in pore water. We first demonstrated the capacity of the DFC to provide insights into CH_4 flux measurement and partitioning and then used it to examine the dependence of CH_4 ebullition fluxes on subsurface bubble dynamics leading to insights into the underlying mechanisms regulating CH_4 ebullition in northern peatlands.

2. Methods

2.1. Sample Collection and Preparation

A peat monolith (approximately 394 × 241 × 330 mm, surface area 0.095 m^2) was extracted on November 2012 from the surface of a lawn dominated by *Sphagnum* spp. and low shrub cover in Caribou Bog, a large, multiunit freshwater peatland complex in Maine [*Comas et al.*, 2008]. The total peat depth at this collection site was previously measured by GPR and estimated to be about 6 m [*Comas et al.*, 2008]. Vegetation on the surface of the monolith was left intact and consisted mainly of *Sphagnum capillifolium* and *Chamaedaphne calyculata*. The monolith was first removed from the field by inserting a mold of the same size (394 × 241 × 350 mm) as the container used to hold the monolith (see below) into the ground and subsequently cutting and pulling back the surrounding peat, and cutting the base of the mold with a machete. The monolith was then placed into a temporary holder, filled by in situ peat water to the peat surface, and transported back to the laboratory.

The monolith was pushed out from the mold into a container made of 10 mm thick transparent acrylic plastic. The exterior walls of the container were entirely covered by black tape to prevent penetration of light and heat. Three pore water sampling ports were drilled vertically into one side of the container at 57 mm, 127 mm, and 197 mm below the peat surface, defining upper, middle, and lower layers of the peat monolith (Figure 1). The width of each layer was 70 mm. Three pore water samplers constructed from PVC pipe (1.58 mm inner diameter) and fitted with a three-way stopcock were horizontally inserted into the ports. Before the start of experiment, the peat monolith was maintained at room temperature (approximately 22–24°C), and distilled water was periodically sprayed onto the peat surface to maintain saturated anaerobic conditions in the peat.

2.2. DFC Setup and Flux Calculation

The DFC is a technique that has been developed to continuously measure earth-atmosphere fluxes of various compounds including CO_2 and CH_4 [*Lai et al.*, 2012]. In contrast to the CSC technique, the DFC is designed to maintain a constant flow of outside air through the chamber enclosing the areas of interest. When the system operates under a dynamic equilibrium, the CH_4 flux (F, mg CH_4 m^{-2} min^{-1}) from the

monolith is determined using the concentration difference between the air entering (C_{in}, mg CH_4 m^{-3}) and leaving (C_{out}, mg CH_4 m^{-3}) the chamber headspace [*Gao and Yates*, 1998],

$$F = \frac{Q}{A} \times (C_{out} - C_{in}), \quad (1)$$

where Q and A are the flow rate of purging air (m^3 min^{-1}) and surface area (m^2) of the peat monolith, respectively.

A DFC requires careful system design to achieve minimal modification of the pressure gradient and CH_4 concentration gradient at the soil-air boundary layer. In this study, we modified the DFC system described in *Mastepanov and Christensen* [2009] by employing an open path fast methane analyzer (FMA, LI-7700, LI-COR Biosciences, Lincoln, NE, USA) positioned in series with the gas chamber (Figure 1a) to determine CH_4 concentration. This DFC system consisted of a flow-through gas chamber (413 × 260 × 325 mm) fitted to the top of the peat container for gas flux measurement (Figure 1a). The chamber was made of 10 mm thick transparent acrylic plastic with a headspace volume of 0.035 m^3. Inflow (25 mm inner diameter and 0.04 m length) and outflow (25 mm inner diameter and 0.5 m length) air ducts, a gas sampling port, and a standpipe for regulating the water table of peat monolith were installed (Figure 1a). A constant flow (0.0047 m^3 min^{-1}) of ambient laboratory air, maintained by a vacuum pump and vacuum regulator, was used as the purging flow (Figure 1a). This flow rate resulted in a mean residence time of air in the chamber of 7.5 min. The combination of low flow resistance at the inflow duct and moderate purging flow rate may keep the pressure difference between the chamber and the laboratory within the range of a few pascal to a few tenths of a pascal during the DFC measurements (see Text S1 in the supporting information for more details about the pressure difference). The chamber headspace was well-mixed using a small low-speed fan (~0.5 m s^{-1}) placed 292 mm above the peat surface and facing downward toward the peat surface (Figure 1a). The continuous measurement of C_{out} then provides information on CH_4 dynamics in the chamber.

We modified the data acquisition mode of the FMA by enclosing it within the calibration shroud provided by the manufacturer, resulting in a closed inner cell (V_{cell}, 0.009 m^3) as the terminal space for CH_4 analysis. After leaving the gas chamber, the purging air flows into the inner cell at the same flow rate as applied to the gas chamber. By assuming complete mixing in the inner cell, a CH_4 mass balance can relate C_{out} to CH_4 concentrations recorded by the FMA in the inner cell (C_{cell}, mg CH_4 m^{-3}),

$$V_{cell} \times \frac{dC_{cell}}{dt} = Q \times (C_{out} - C_{cell}) \quad (2)$$

C_{out} can then be obtained from the time series of C_{cell} collected at 5 Hz.

2.3. CH_4 Concentration Corrections

The determination of C_{in} and C_{out} by the FMA is affected by variations of temperature and water vapor via thermal expansion and water vapor dilution. In addition, temperature, pressure, and water vapor density in the inner cell impact concentration measurements by shifting the spectroscopic light absorption of the FMA [*McDermitt et al.*, 2011]. In order to take these effects into account, we measured temperature, atmospheric pressure, and relative humidity of the chamber headspace every 10 min (RHT50, Extech Instruments, USA) beside the outflowing duct in the gas chamber. Another environmental sensor was installed in the laboratory to measure ambient conditions for comparison. As the FMA was connected to the gas chamber for more than 5 days per individual experiment (see below), it is reasonable to assume that the inner cell quickly reached a dynamic equilibrium with the gas chamber in terms of water vapor density. The raw bulk CH_4 concentration data were corrected by using 10 min averaged water vapor densities converted from the relative humidity of the chamber headspace, and FMA measured temperature and pressure according to the Webb-Pearman-Leuning (WPL) corrections [*Webb et al.*, 1980] and spectroscopic correction [*McDermitt et al.*, 2011] prior to C_{out} inversion. Figure 2a summarizes the sequence of the data correction and calculation steps described above, and Figure 2b shows a typical flux data set obtained from the DFC system.

2.4. Flux Partitioning and Ebullition Identification

Recent studies suggest that in peatlands, CH_4 ebullition can occur in a steady manner over time frames of minutes to hours [*Coulthard et al.*, 2009]. In some studies, diffusion, plant-mediated transport, and steady ebullition are collectively defined as steady emission, while ebullition occurring in short-lived bursts or episodes where fluxes are generally much higher and more variable than background steady fluxes is termed episodic ebullition [*Green and Baird*, 2012]. We follow such definitions to partition measured total CH_4 fluxes in this study.

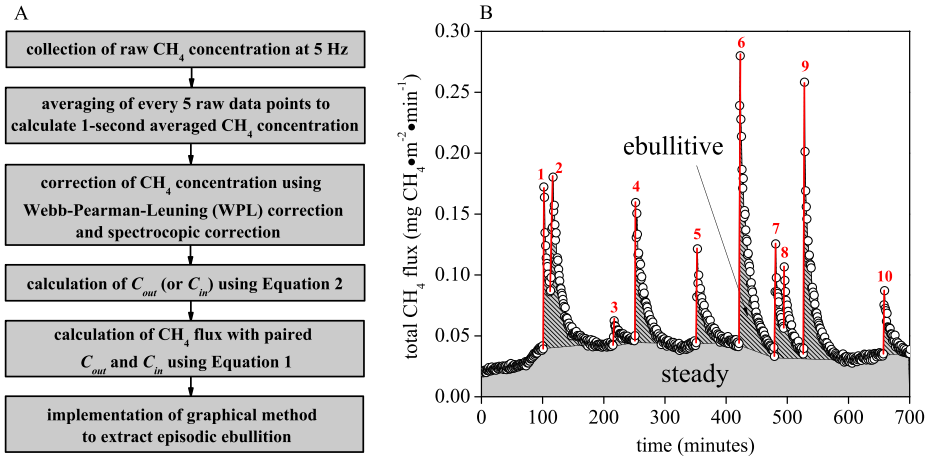

Figure 2. (a) Flowchart of procedure for data correction, calculation, and extraction. (b) Example of the dynamics of CH_4 flux observed using DFC. Steady flux (solid gray shading) and episodic ebullition flux (striped shading) were separated and identified using a graphical model. Ten ebullitive CH_4 releases were identified (straight red lines). The flux data shown as the example were collected at the nighttime of day 4, week 3.

Using the DFC system, the frequency of episodic ebullition during a specific time period can be determined by visual counting of flux peaks in flux time series data (Figure 2b). Ideally, episodic ebullition fluxes can be accurately separated out from steady fluxes due to substantial amounts of CH_4 contained in biogenic gas bubbles [*Tokida et al*., 2005]. However, by using a purging flow rate that causes no significant pressure deficit in the gas chamber, it is unavoidable that full detection of ebullition-derived CH_4 by the DFC system lags behind the instant occurrence of ebullition [*Christensen et al*., 2003]. The calculated fluxes using equations (1) and (2) are thus apparent fluxes rather than instantaneous CH_4 emission rates from the peat monolith. In this sense, episodic ebullition fluxes are best isolated from the baseline steady fluxes by integrating areas under flux peaks [*Panikov et al*., 2007] (Figure 2b).

Methods exist to statistically identify a baseline in a time series and quantitatively integrate area under peaks, e.g., chromatographic algorithms. However, these methods may not be easily applied in this case where the baseline representing steady fluxes has a varying nature [*Panikov et al*., 2007]. By using a similar flow-through system, *Christensen et al*. [2003] defined steady baselines visually with a fixed flux rate for individual data sets. In this study, we adopted a simple graphical model that mimics the hydrological approach for identifying base flow and stormflow in stream hydrographs [*Dingman*, 1994]. We defined the baselines by tracking the smooth variation in flux until first arrival of a peak and identifying the point at which the peak returned to a steady state, such that the baseline was set as a straight line under the peak (Figure 2b). Calculated total CH_4 fluxes were first plotted and normalized to a standard axis format. The flux graphs were then imported into ImageJ for calculation of areas defining total flux and steady fluxes, respectively (Figure 2b). The difference between total flux and steady fluxes gives the integrative episodic ebullition flux over the time period of interest (Figure 2b).

Similar to other flow-through systems (e.g., inline membrane probes for in situ measurement of pore water chemistry [*Mastepanov and Christensen*, 2009]), the difference between peak height and baseline level is a good approximation of CH_4 content in individual episodic events. Once integrated episodic ebullition flux for a specific time period was extracted, we graphically measured the peak height for all individual ebullition peaks included in this time period (Figure 2b), which were further summed up to calculate the total length that corresponds to the total amount of episodic CH_4 ebullition. Individual peak heights were then converted to ebullitive CH_4 release for each episodic ebullition event according to their proportion of the total length. All original flux data showing the defined baseline and identified peak heights are provided in the supporting information.

2.5. CSC Measurements

The gas chamber of the DFC system was modified for CSC measurements of steady fluxes by closing the inflow and outflow holes with fittings and extending the water resupply tube to be a vent tube for pressure balance. For each CSC measurement, a 30 min chamber closure time was adopted; seven 30 mL gas samples

were taken from the top sampling port at a 5 min time interval after chamber closure and injected into prevacuumed 20 mL vials for gas chromatograph (GC, Shimadzu, GC-8A, Japan) analysis. Detailed GC configuration was documented in *Treat et al.* [2007]. Linear regressions were performed on each set of CH_4 concentration series to calculate flux. The CSC flux measurement was accepted if the determination coefficient of linear regression (R^2) was larger than 0.90.

2.6. GPR Measurements

The theory and methods employed to use GPR to characterize gas bubble dynamics in peat soils have been documented elsewhere [e.g., *Comas et al.*, 2008]. In this work, we modified a laboratory GPR system and data acquisition protocol initially used by *Comas and Slater* [2007], improving the accuracy of gas content estimates by replacing reflection-based measurements with transmission measurements.

A Mala-RAMAC GPR system equipped with a pair of 1.2 GHz shielded antenna was used to compute the velocity of electromagnetic (EM) waves in the upper, middle, and lower layers of the peat monolith (three lines as shown in Figure 1a). Three horizontal positions spaced 0.1 m apart were used for a GPR measurement in each layer. EM waves were transmitted across the monolith, and direct wave travel times, complete with reciprocal data for each location, were recorded. The velocity (v) of the EM wave in peat is calculated using the known distance that the EM wave traveled (i.e., across the length of the peat container). Assuming a low-loss medium [*Comas and Slater*, 2007; *Parsekian et al.*, 2012], v can then be simply converted to the bulk relative permittivity of the peat ($\varepsilon_{r(b)}$),

$$\varepsilon_{r(b)} = \left(\frac{c}{v}\right)^2, \tag{3}$$

where c is the EM wave velocity in a vacuum (3×10^8 m s^{-1}).

The strong contrast in relative permittivity between air ($\varepsilon_{r(a)} = 1$) and water ($\varepsilon_{r(w)} = 79$ at laboratory temperature of 23°C) forms the basis for using measurements of $\varepsilon_{r(b)}$ to determine gas content in peat soils. A multiphase dielectric mixing model variant of the Complex Refractive Index Model was applied to estimate gas content [*Parsekian et al.*, 2012],

$$\varepsilon_{r(b)}{}^{\alpha} = \theta\varepsilon_{r(w)}{}^{\alpha} + (1 - \phi)\varepsilon_{r(s)}{}^{\alpha} + (\phi - \theta)\varepsilon_{r(g)}{}^{\alpha}, \tag{4}$$

where $\varepsilon_{r(s)}$ is relative permittivity of the solid phase assumed here as 2 [*Comas and Slater*, 2007], θ is the water content, ϕ is porosity, and α is an empirical coefficient related to the orientation of the electromagnetic waves to the peat particles. The term $\phi - \theta$ is the volumetric gas content of the peat. In this study, we set the value of $\alpha = 0.33$ as previously determined empirically for Caribou Bog peat samples [*Parsekian et al.*, 2012]. We assume that porosity did not change throughout the experiment due to the container wall preventing horizontal peat deformation [*Comas and Slater*, 2007] and limited vertical peat deformation (see below). Thus, the porosity measured at the end of the incubation (see below) was used in equation (4) to back calculate gas content for the entire study.

2.7. Measurement of Peat Surface Elevation

Surface elevation of the peat monolith was monitored using the method documented in *Comas and Slater* [2007]. In brief, a cover of the same size as the peat surface area, made of plastic perforated sheet, was positioned above the peat surface during the measurements. Seven evenly spaced lines were set longitudinally on the cover with eight measurement holes equally spaced along each line. The distance between the bottom of the cover and the peat surface was measured at each hole using an elevation rod and a caliper. The peat surface elevation was calculated by subtracting this distance from a fixed reference at the bottom of the peat monolith. Estimated maximum measurement error was 2 mm [*Comas and Slater*, 2007].

2.8. Dissolved CH_4 Concentration Measurements

To measure the dissolved CH_4 concentrations in pore water, 2 mL of pore water was collected with a syringe from the samplers in the upper, middle, and lower layers, respectively, and injected into an 8 mL vial filled with ambient air. The vials were then shaken vigorously for 15 min to equilibrate CH_4 between the headspace and water phase. The CH_4 concentration in the headspace of the vial and two replicates of ambient air were2 determined by GC, and the original dissolved concentration was reconstructed using the headspace

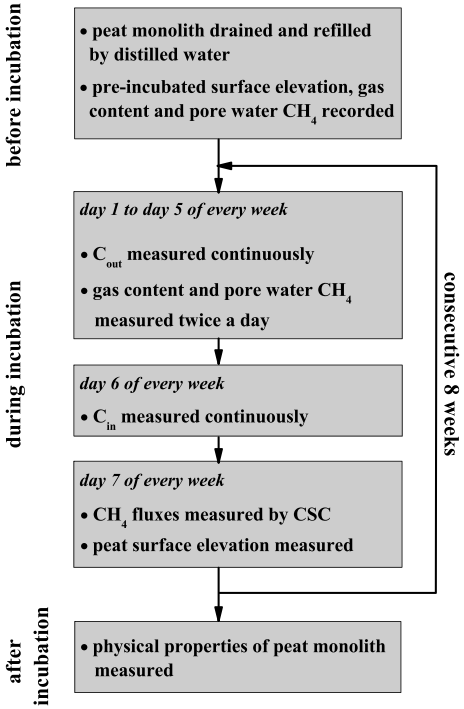

Figure 3. Flowchart showing experimental procedure before, during, and after incubation.

concentrations, the ambient CH_4 concentration, the volumes of the headspace and water phase, and temperature-corrected Bunsen solubility coefficient [*Wiesenburg and Guinasso*, 1979].

2.9. Modeling CH_4 Diffusion Fluxes From the Peat

Methane diffusion fluxes across the soil surface can be theoretically calculated from the CH_4 concentration gradient within the soil using Fick's first law of diffusion [*Nielson et al*., 1984]. In flooded peat, CH_4 diffusion occurs in both air-filled and water-filled pore spaces [*Stephen et al*., 1998]. In this study, CH_4 diffusion fluxes from the peat monolith were modeled using Fick's first law with model coefficients specifically derived for flooded soil containing gas bubbles (equation (5)),

$$F = D_e \frac{\partial C_b}{\partial z} \approx D_e \frac{C_b}{\partial z}, \tag{5}$$

$$D_e \approx \left[\frac{(\varphi+\theta)\sqrt{D_a D_w}}{\varphi\sqrt{D_w}+\theta\sqrt{D_a}}\right]^2, \tag{6}$$

$$C_b = \varphi C_a + \theta C_w = \left(\frac{\varphi}{\alpha_b}+\theta\right) C_w, \tag{7}$$

where D_e is the effective bulk diffusion coefficient and can be expressed as a function of the CH_4 diffusion coefficients in free air (D_a) and water (D_w), gas content (φ), and water content (θ) of the peat medium (equation (6)) [*Nielson et al*., 1984; *Stephen et al*., 1998]. The term $\partial C_b/\partial z$ is the gradient of bulk CH_4 concentration over depth z to the water table. By assuming that equilibrium in the gas-pore water system can be reached rapidly and obeys Henry's law, C_b can be calculated using measured φ, θ, dissolved CH_4 concentration (C_w), and Bunsen solubility coefficient for CH_4 (α_b) according to equation (7) [*Stephen et al*., 1998]. In the calculations using equation (5) a simplification was made because C_b in peat is much higher than the equilibrated CH_4 concentration at the water table [*Reid et al*., 2013]. All diffusion and solubility coefficients used in this study were corrected for temperature.

An important boundary condition on Fick's first law is that the concentration gradient in soil has to be taken in the direction where it is steepest [*Rothfuss and Conrad*, 1998]. Gas bubbles affect CH_4 concentration gradients in flooded soils and thus CH_4 diffusion modeling by (1) resulting in a three-dimensional uneven structure of CH_4 gradients in which the concentration isopleths follow the surface of trapped gas bubbles [*Rothfuss and Conrad*, 1998] and (2) increasing dissolved CH_4 concentrations in shallower peat via redissolution during their migration toward the surface [*Tang et al*., 2010]. As a result, the distribution of CH_4 in the flooded soil profile is highly variable even in layers right below the water table [*Panikov et al*., 2007], and any choice of depth in the calculation of a concentration gradient will be arbitrary. For simplicity, we used average values of the three layers and set the lower boundary of the concentration gradient at the middle layer to model CH_4 diffusion flux for each experimental day.

2.10. Experimental Procedure

The experimental procedure is summarized in Figure 3. In order to examine the evolution of gas bubble buildup and its association with ebullition fluxes, the peat monolith was carefully drained 2 days before the incubation and then slowly rewetted with distilled water from the bottom pore water sampling port until the water table was 2 cm below the peat surface to encourage a low initial CH_4 level and gas content in peat. One set of GPR measurements, one round of pore water sampling, one set of surface elevation measurements, and three sets of CSC flux measurements were taken immediately after the rewetting to establish preincubated conditions.

Eight consecutive weeks of incubation for CH_4 ebullition monitoring began on 26 March 2013. A florescent light was set up above the gas chamber for simulating a 12 h day/night cycle with a daytime photosynthetically

active radiation of 17.2 J m^{-2} s^{-1} at the peat surface and providing additional heating that enhanced the amplitude of temperature variation in the gas chamber (Figure 1a). During the entire incubation, the water table was maintained at its initial level by replenishment with 30 to 60 mL distilled water through the water filling tube for every 12 h coincident with the diel transitions. For every experimental week, the DFC system was started 12 h before collecting continuous CH_4 flux data to allow the system to reach a dynamic equilibrium. Methane concentration of the outflow (C_{out}) was continuously measured from day 1 to day 5 (Monday to Friday, 120 h, 5 day/night cycles) under continuous chamber closure. GPR and pore water sampling on the three layers were conducted twice a day during the daytime condition. Ambient CH_4 concentration (C_{in}) was continuously measured over 24 h on day 6 (Saturday) after the disconnection of FMA from the gas chamber. Eight C_{in} data sets acquired were averaged to get one 24 h data set with 1 min resolution for the flux calculation of each experimental day. On day 7 (Sunday), three sets of CSC flux measurements were taken during the daytime condition, followed by one set of surface elevation measurements.

After 8 weeks of incubation, three replicate samples were extracted from the upper, middle, and lower layers of the monolith, respectively, by cutting from the surface. The humification degree, stratum characteristics, bulk density, and porosity were measured using a weight loss on drying procedure previously used by *Comas and Slater* [2007].

2.11. Uncertainty Analysis and Data Statistics

Uncertainties in calculated CH_4 fluxes using equation (1) may arise from the unsynchronized samplings of C_{in} and C_{out} and the use of averaged C_{in} if the variation of C_{in} was large on a day-to-day basis. These uncertainties may possibly propagate to the partitioned steady and ebullition CH_4 fluxes. Gaussian error propagation was used to estimate the uncertainty in calculated apparent CH_4 fluxes [*Taylor*, 1997]. The uncertainty of C_{in} with 1 min resolution is set as the standard deviation of C_{in} calculated using all eight data sets. The uncertainty of C_{out} was set to the noise of the instrument under ambient CH_4 concentrations (±0.25%) measured in the laboratory. The error in Q was estimated from the standard deviation of the measured flow rate using a gas flow meter. The error in A was propagated from the dimension measurements (~2 mm) and geometrical calculations. More details regarding the uncertainty calculations are in Text S2 in the supporting information.

The corrections and calculations of all CH_4 fluxes and associated uncertainties were performed in MATLAB (Mathworks, Natick, MA, USA), and all statistical tests were performed using SPSS (SPSS Inc., ISM corp., Armonk, NY, USA). A one-way analysis of variance followed by Fisher's least significant difference (LSD) test for pairwise comparison was used to determine significant differences between independent variables. Simple linear regression and Pearson's Correlation Coefficient were used to detect significant relationships among independent variables.

3. Results

3.1. Peat Properties

The von Post humification test indicated that the upper layer of the monolith was undecomposed (H2), while the middle and lower layers were slightly decomposed (H3–H4). Below the upper layer (~92 mm below the peat surface), *Sphagnum* accumulated with slightly decomposed branches, stems, and variable amounts of woody material (Figure 1b). Bulk density was found to be 0.052 g cm^{-3}, 0.065 g cm^{-3}, and 0.078 g cm^{-3} for the upper, middle, and lower layers, respectively. Porosities for the upper, middle, and lower layers were 0.96, 0.95, and 0.94, respectively.

3.2. Incubation Conditions

The temperature in the gas chamber exhibited significant diel patterns (Figure 4). Averaged 10 min temperatures were 23°C to 24°C during nighttime, increasing to 26°C to 27°C when the florescent light was on. Regardless of the diel shifting, temperatures during daytime and nighttime were stable. While relative humidity exhibited a reverse diel pattern to temperature, relative humidity was always greater than 95% in the gas chamber. During the entire incubation, the peat monolith experienced a range of atmospheric pressure from 100.2 kPa to 103.5 kPa. Averaged 1 min C_{in} ranged from 1.31 mg CH_4 m^{-3} to 1.46 mg CH_4 m^{-3} (Figure 4). While daytime C_{in} was relatively stable and consistent among the experimental weeks, nighttime C_{in} varied more, especially in the later period, and did not follow any predictable temporal pattern (Figure S1 in the

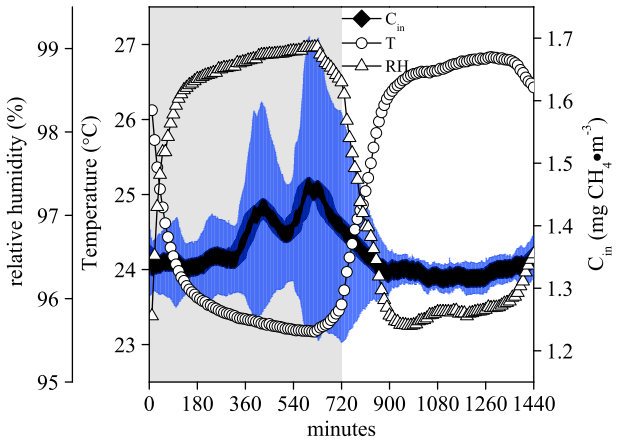

Figure 4. Averaged 10 min temperature and relative humidity in gas chamber and averaged 1 min C_{in} for every minute. Standard deviation of C_{in} is shown as error bars. Shaded area denotes nighttime.

supporting information). However, nighttime C_{in} fluctuated at a very slow rate and with a magnitude much smaller than C_{out}, especially in the later phase of the experiment (Figure S2 in the supporting information). Occasional changes in the settings of the air conditioning and ventilation systems of the building may have caused the C_{in} fluctuations. More details regarding the C_{in} fluctuations are in Text S2 in the supporting information.

3.3. Peat Surface Elevation, Gas Content, and Dissolved CH_4 Concentrations

Figure 5a shows the changes in surface elevation against the preincubation elevation as a function of time. The surface elevation decreased to below the initial elevation by the end of week 1 and then generally increased toward the end of the incubation. However, averaged change in surface elevation measured in week 8 was only 6 mm, corresponding to about 2% of the averaged surface elevation measured before the incubation, indicating that the vertical peat deformation was limited throughout the incubation.

Preincubation gas content measured by GPR for the upper, middle, and lower layers was 0.04 $m^3\ m^{-3}$, 0.06 $m^3\ m^{-3}$, and 0.07 $m^3\ m^{-3}$, respectively. Gas content of the middle and lower layers, 0.11 ± 0.02 $m^3\ m^{-3}$ (0.06 to 0.14 $m^3\ m^{-3}$) and 0.13 ± 0.02 $m^3\ m^{-3}$ (0.08 to 0.15 $m^3\ m^{-3}$) on average, generally increased from

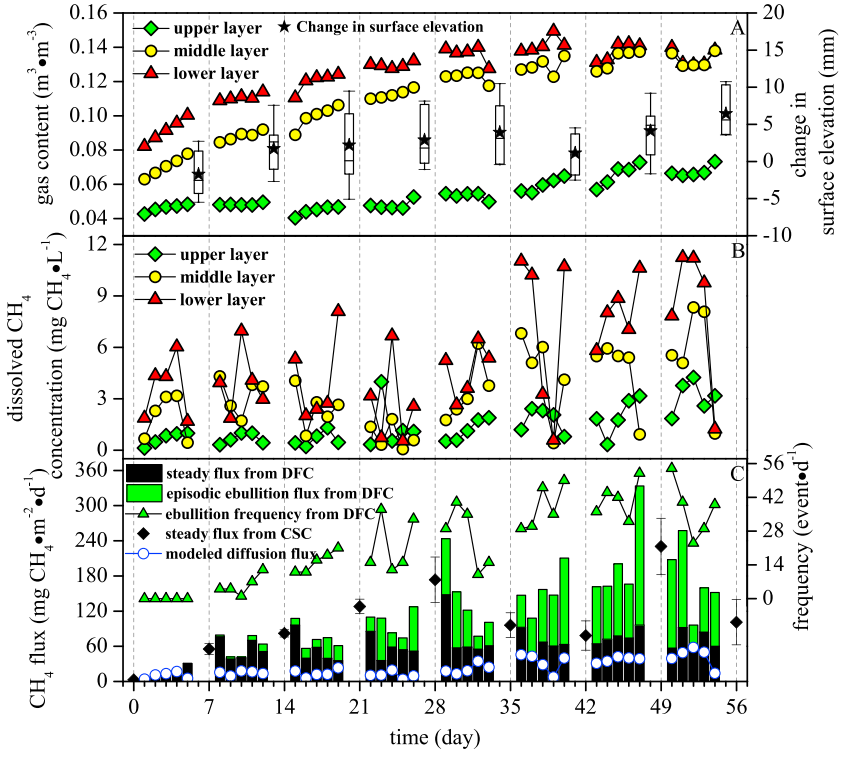

Figure 5. (a) Gas content and change in surface elevation measured at different measurement lines, (b) dissolved CH_4 concentrations, and (c) steady and ebullition fluxes, ebullition frequency, and modeled diffusion fluxes as a function of time. In Figure 5a, the center line and box extent denote the median and 25th and 75th percentiles; error bars denote maximum and minimum values; asterisks denote mean value.

the start of the experiment with a higher rate of increase during weeks 1 to 5 (Figure 5a). Fisher's LSD test indicated that gas content of the lower layer was significantly higher than the middle layer and the upper layer ($P < 0.01$ in all comparisons).

Preincubation dissolved CH_4 concentrations were 0.075 mg CH_4 L^{-1}, 0.003 mg CH_4 L^{-1}, and 0.007 mg CH_4 L^{-1}, respectively, for the upper, middle, and lower layers. Dissolved CH_4 concentrations of the middle and lower layers increased rapidly after the experiment started but exhibited strong variability throughout the experiment with the largest concentration reduction (8.5 mg CH_4 L^{-1}) in the lower layer (Figure 5b). Despite the higher variability in concentration, the lower layer of the monolith had significantly higher dissolved CH_4 concentrations (5.3 ± 3.3 mg CH_4 L^{-1}) than the middle layer (3.3 ± 2.2 mg CH_4 L^{-1}) and the upper layer (1.4 ± 1.1 mg CH_4 L^{-1}) ($P < 0.01$ in all comparisons). A positive correlation between dissolved CH_4 concentration and gas content was detected in the middle layer ($R^2 = 0.40$, $P < 0.05$) and upper layer ($R^2 = 0.65$, $P < 0.01$).

3.4. Measured and Modeled CH_4 Fluxes

Twenty-four out of 27 CSC flux measurements met the linearity criteria with $R^2 > 0.90$ (Figure S4 in the supporting information). Preincubation CSC CH_4 flux was 2.7 ± 0.4 mg CH_4 m^{-2} d^{-1} (Figure 5c). Throughout the experiment, CSC CH_4 fluxes ranged from 50.9 ± 8.7 mg CH_4 m^{-2} d^{-1} to 212.2 ± 44.3 mg CH_4 m^{-2} d^{-1} with an average of 97.0 ± 61.1 mg CH_4 m^{-2} d^{-1} (Figure 5c).

Modeled CH_4 diffusion fluxes from the peat monolith ranged from 3.5 mg CH_4 m^{-2} d^{-1} to 53.4 mg CH_4 m^{-2} d^{-1} (Figure 5c) with an average of 21.2 ± 13.7 mg CH_4 m^{-2} d^{-1}. Modeled CH_4 diffusion fluxes had significant positive correlations with all measured gas content and dissolved CH_4 concentrations of the three layers (R^2 ranging from 0.50 to 0.91; $P < 0.01$ for all cases).

Daily integrated total CH_4 fluxes measured by DFC ranged from 3.8 mg CH_4 m^{-2} d^{-1} to 333.6 mg CH_4 m^{-2} d^{-1}. The average uncertainty in total CH_4 flux for the entire experiment was ±12.2%. The C_{in} fluctuations constituted the majority of uncertainty in total CH_4 flux (see Text S2 in the supporting information). The uncertainty in total CH_4 fluxes propagated to partitioned steady fluxes but did not bias the quantification of episodic fluxes and ebullitive releases using the graphical method (Figure S3 and Table S2 in the supporting informaton). Additional uncertainty in both steady fluxes and episodic ebullition fluxes may arise from the assumptions inherent to the graphical method (see below). Hereafter, only mean values of CH_4 fluxes and ebullitive CH_4 releases are shown. Uncertainties associated with the CH_4 fluxes from the DFC measurements are given in Table S3 in the supporting information. All raw CH_4 flux data measured by DFC and flux partitioning using the graphical method are shown in Figures S5–S12 in the supporting information.

Steady fluxes (Figure 5c), ranging from 3.8 mg CH_4 m^{-2} d^{-1} to 148.1 mg CH_4 m^{-2} d^{-1}, 58.5 ± 27.3 mg CH_4 m^{-2} d^{-1} on average, gradually increased in week 1 and then did not differ significantly after week 1 when compared on a weekly basis ($P > 0.05$ for all comparisons). A difference test indicates that the steady fluxes from DFC were significantly higher than modeled CH_4 diffusion fluxes ($P < 0.01$). Episodic ebullition did not occur until the first day of week 2. Episodic ebullition fluxes, ranging from 1.8 mg CH_4 m^{-2} d^{-1} to 237.3 mg CH_4 m^{-2} d^{-1}, 56.9 ± 55.1 mg CH_4 m^{-2} d^{-1} on average, were then recorded, with fluxes generally increasing toward the end of the experiment. Episodic ebullition fluxes for weeks 6, 7, and 8 were significantly higher than those for weeks 2, 3, and 4 ($P < 0.01$ for all comparisons). After averaging steady fluxes and episodic ebullition fluxes measured within the same week and averaging CSC fluxes obtained before and after every experimental week, we found that steady fluxes from DFC were significantly lower than CSC fluxes ($P < 0.05$) but CSC fluxes were not significantly different from total fluxes from DFC ($P > 0.05$). Ebullition frequency followed the same temporal pattern as ebullition fluxes ($R^2 = 0.91$, $P < 0.01$) with the first day of week 8 having the highest frequency (54 events d^{-1}).

Figures 6a and 6c show the relationships between episodic ebullition fluxes, ebullition frequency, and gas content of the three layers. Episodic ebullition fluxes increased dramatically when gas content of the middle and lower layers leveled off at 0.14 m^3 m^{-3}. Linear relationships between ebullition frequency and gas content for both of these layers tended to be stronger than between ebullition fluxes and gas content. In contrast, positive but weak relationships exist between dissolved CH_4 concentrations and both episodic ebullition flux and frequency for the upper and lower layers (Figures 6b and 6d).

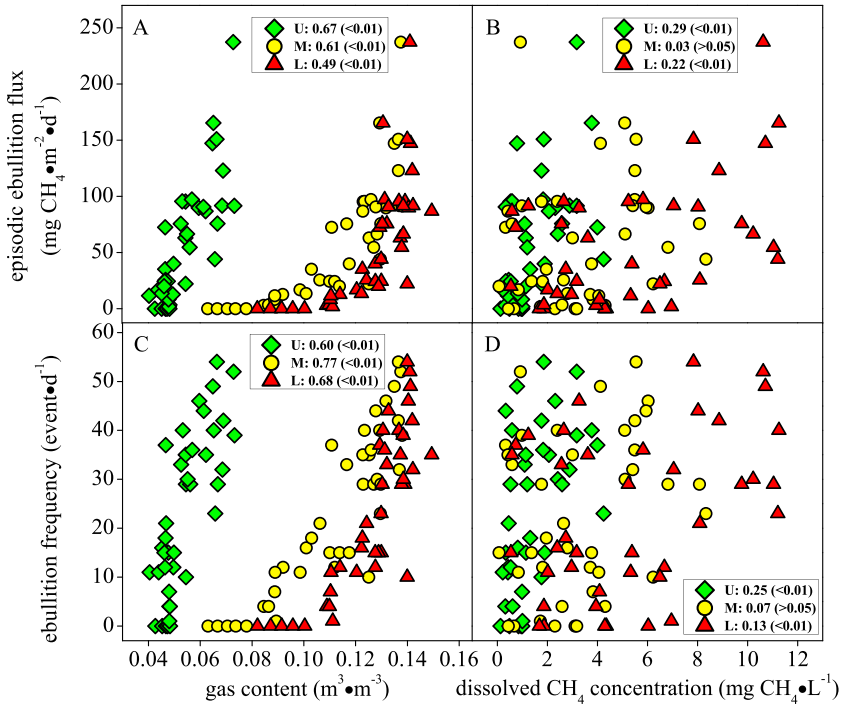

Figure 6. (a–d) Relationships between gas content, dissolved CH_4 concentration, ebullition fluxes, and ebullition frequency for three layers. Letters "U," "M," and "L" in the figure represent upper, middle, and lower layers, respectively. R^2 and P values of the linear regressions are shown in the legend and in brackets, respectively.

There were a total of 926 events of ebullitive CH_4 release, ranging from 0.01 mg CH_4 to 4.36 mg CH_4, observed in this study. The frequency distribution of ebullition magnitude exhibit a strong positive skew, with 95% of ebullitive CH_4 releases being below 0.6 mg CH_4 (Figure 7). Based on this frequency distribution, ebullitive CH_4 releases within each class were summed up and then converted to the overall episodic ebullition flux by dividing the peat surface area and the time interval covering all episodic ebullition events (35 days). Ebullitive CH_4 releases in the range of 0.2 to 0.3 mg CH_4 contributed the highest overall episodic ebullition flux, followed by ebullitive CH_4 releases in the range of 0.1 to 0.2 mg CH_4 (Figure 7). Ebullition occurred more frequently at daytime than at nighttime over the entire experiment ($P < 0.01$) (Figures 8a and 8b). However, larger ebullitive CH_4 releases occurred during nighttime when temperature was lower during weeks 6 to 8 ($P < 0.01$) (Figures 8a and 8b). The cumulative ebullitive CH_4 releases, calculated for every 12 h in each experimental day, were significantly and negatively related to changes in atmospheric pressure, defined as the difference between averaged atmospheric pressure for any 12 h and that of the previous 12 h, especially in weeks 6 to 8 ($P < 0.01$ for all cases) (Figures 8c and 8d). A tendency for the largest 5% of ebullitive CH_4 releases to occur with large drops in atmospheric pressure is evident, especially in weeks 6 to 8 (Figures 8c and 8d).

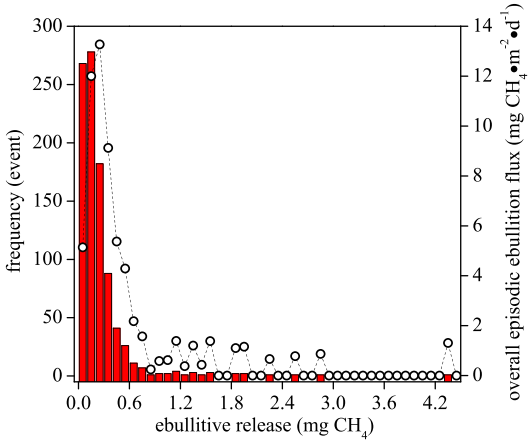

Figure 7. Frequency distribution of ebullition CH_4 releases (bars) and overall episodic ebullition flux for each class of ebullitive release (dots) observed over the entire study period ($n = 926$).

4. Discussion

4.1. Reliability of DFC for Continuously Monitoring of CH_4 Ebullition

Using the DFC system, successful measurement of CH_4 fluxes relies on careful design of the chamber

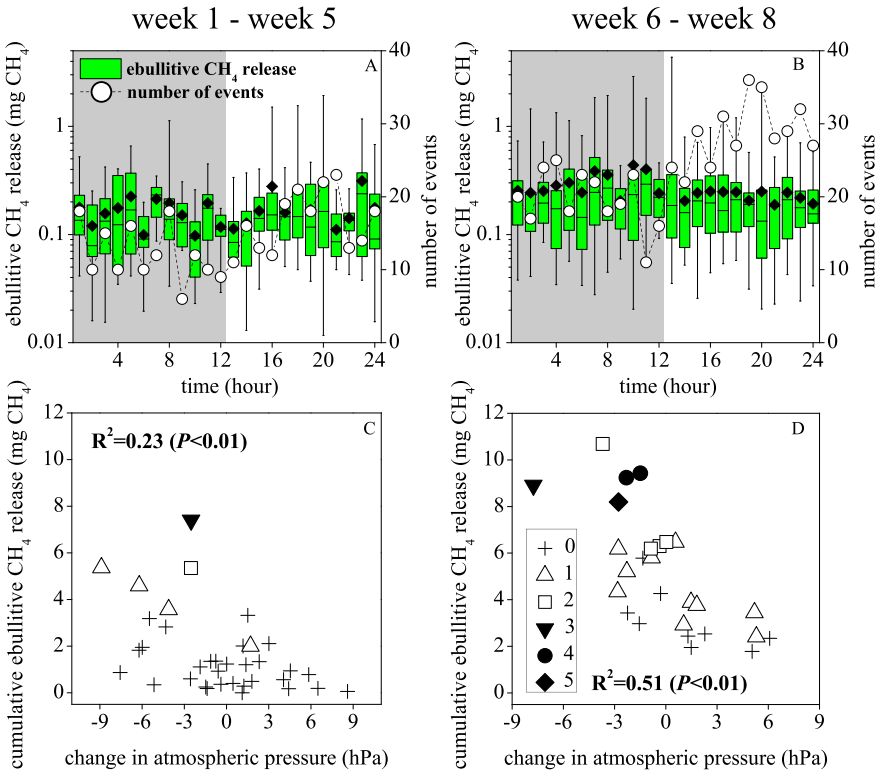

Figure 8. (a, b) Ebullitive CH_4 releases observed every experimental hour for weeks 2–5 and weeks 6–8, respectively. The box shows the distance between the 25th and 75th percentiles, with the 50th percentile shown as a line. The error bars denote the minimum and maximum, and the filled diamond denotes the mean. The shaded area represents nighttime. Note log scale for *y* axis. (c, d) Relationships between cumulative ebullitive CH_4 release and change in atmospheric pressure for weeks 2–5 and weeks 6–8, respectively. The number of the largest 5% of ebullitive CH_4 releases in Figures 8c and 8d is indicated with different symbols (legend in Figure 8d). Linear regression R^2 and *P* values are shown.

system and experimental procedures to minimize disturbance induced by the chamber closure [*Hutchinson et al*., 2000]. In this study, artificial pressure differences between chamber and ambient atmosphere, which might potentially induce artifacts in measured CH_4 fluxes [*Gao and Yates*, 1998], were minimized to be within the range of a few pascal to a few tenths of a pascal by reducing the flow resistance at the inflowing duct and using a moderate flow rate (Table S1 in the supporting information). It may also be argued that the natural CH_4 gradient at the air-peat interface was reduced by long-term closure of the gas chamber and excess accumulation of ebullition-derived CH_4 such that the natural regime of steady emission was disturbed [*Lai et al*., 2012]. Averaged bulk CH_4 concentration of the peat monolith calculated by equation (8) (2.26 to 33.76 mg CH_4 L^{-1}) was at least 3 orders higher than dissolved CH_4 concentration (0.04 to 0.19 μg CH_4 L^{-1}) equilibrating with observed daily averaged C_{out} (1.40 to 5.82 μg CH_4 L^{-1}). In contrast to other types of soil, the combination of high porosity and essentially unlimited biogenic CH_4 production potential in peat results in a large CH_4 reservoir and high ebullition potential for peat. As a result, the disturbance of the natural gas exchange regime was likely minimal during the DFC measurements.

In this study, total CH_4 fluxes measured by DFC are subject to uncertainty resulting from the temporally sparse measurements of C_{in} (Table S3 in the supporting information). However, even if the largest C_{in} fluctuation was assumed in the flux calculation, the quantified episodic ebullition fluxes and ebullitive CH_4 releases using the graphical method were still unaffected (Figure S3 and Table S2 in the supporting information). Two factors may contribute to the insensitivity of episodic ebullition fluxes to the uncertainty in total CH_4 fluxes [*Mastepanov and Christensen*, 2009]. First, gas bubbles in peat contain a large concentration of CH_4 so that the magnitude of ebullition-induced C_{out} variations was much larger than that of C_{in} fluctuations or diffusion-induced C_{out} variations, leading to distinguishable ebullition signals in the flux graphs (Figure 2b); second, the episodic nature of CH_4 ebullition together with the fast and continuous chamber

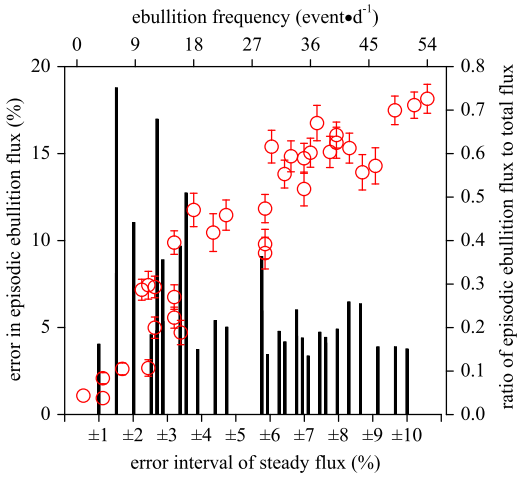

Figure 9. Propagated percentage error in calculated episodic ebullition fluxes using the graphical model (bars) and relationship between ebullition frequency and the ratio of ebullition flux to total flux (dots). Percentage error in episodic ebullition fluxes and the error of flux ratios are taken from Table S3 in the supporting information.

purging ensures a short residence time for ebullition-derived CH_4 [*Pape et al*., 2009], limiting the propagation of baseline uncertainty to the partitioning of episodic ebullition (Figure 2b). However, with a flow rate causing no significant pressure deficit in the chamber, the accumulation of ebullition-derived CH_4 in the gas chamber is inevitable. Potential uncertainty in episodic ebullition fluxes might arise from the assumption that the trend of steady flux is linear when ebullitive CH_4 peaks obscure the steady baseline in the flux graphs (Figure 2b). This uncertainty is inherent to the graphical method and mutual to partitioned steady fluxes and episodic ebullition fluxes. It is reasonable to speculate that the steady baseline can be accurately defined when episodic ebullition is lacking or infrequent, and higher ebullition frequency results in higher uncertainty in defining the baseline. To assess potential uncertainty to partitioned episodic ebullition fluxes, we assigned an arbitrary error level, ranging from ±1% to ±10% of partitioned mean steady flux, proportional to the ebullition frequency, to both steady fluxes, and episodic ebullition fluxes. As shown in Figure 9, when ebullition frequency was higher than 30 events d^{-1} and calculated episodic ebullition fluxes constituted over half of the total flux, the distributions of likely error in calculated episodic ebullition fluxes and their ratios to total CH_4 fluxes are constrained to very narrow ranges, highlighting the insensitivity of episodic ebullition fluxes to the uncertainty in total CH_4 fluxes and assumption of linear baseline, especially during the later phase of the experiment.

When compared on a weekly basis, steady fluxes measured by DFC were significantly lower than fluxes from CSC ($P < 0.05$) but significantly higher than modeled diffusion fluxes ($P < 0.01$) (Figure 5c). The uncertainty in steady flux measurements originating from the C_{in} fluctuations might partially be responsible for the differences (Table S3 in the supporting information). However, even if the highest or lowest steady fluxes from the estimated variation range were assumed (Table S3), the differences between fluxes estimated from the three methods were still significant ($P < 0.05$ for the comparison with CSC fluxes and $P < 0.01$ for the comparison with modeled diffusion fluxes). Due to the dominance of *Sphagnum* species, we can safely assume that plant-mediated CH_4 transport was minimal in this peat monolith [*Stephen et al*., 1998]. Subsequently, the differences between fluxes estimated from these three methods are most likely attributed to steady ebullition from the peat. *Coulthard et al*. [2009] proposed that shallow peat layers are sources of steady CH_4 ebullition that is released to the atmosphere as a continuous stream of relatively small bubbles, causing a linear increase of the CH_4 concentration in CSC headspace over time. However, regardless of the uncertainties in both methods, the large differences in temporal resolution between the CSC and DFC make it difficult to extract valuable information from the comparison of these results. While CSC measurements span 90 min for every experimental week, continuous DFC monitoring, which accounts for considerable temporal variability in the dissolved CH_4 reservoir in peat (Figure 5b), provides a better characterization of temporal variability in CH_4 steady fluxes. In the later phase of our experiment, we observed much larger deviation in the replicate CSC measurements (Figures 5c and S4 in the supporting information). It is possible that the observed higher CSC fluxes (e.g., those measured after week 4, week 7, and week 8; Figures 5c and S4) might include time periods of active steady ebullition. If only the lowest values of replicate measurements are used to represent CSC fluxes after week 4, week 7, and week 8, no significant difference was found between CSC fluxes and mean steady fluxes from DFC ($P > 0.05$).

Therefore, we calculated the steady ebullition fluxes as the difference between steady fluxes from DFC and modeled diffusion fluxes (Figure 10). Uncertainty for each calculated flux is given in Table S3 in the supporting information. Episodic ebullition constituted 0 to 73 ± 3% of the total fluxes with an average of

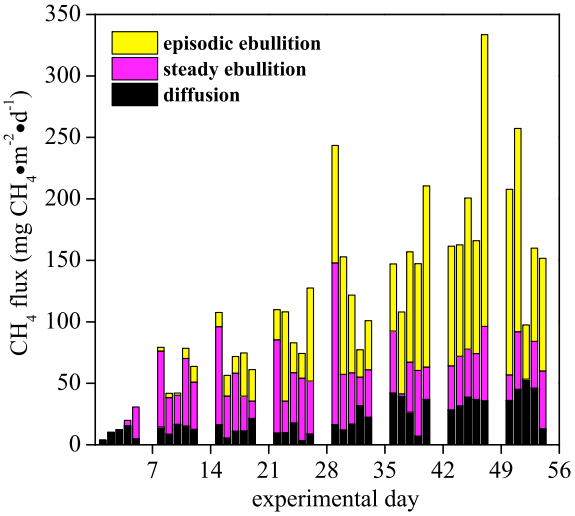

Figure 10. Partitioned diffusion flux, steady ebullition flux, and episodic ebullition flux for each experimental day.

38 ± 24% throughout the experiment (Figure 10 and Table S3), being consistent with previous findings of 17%–52% using similar flow-through systems at the same scale [*Christensen et al*., 2003]. Steady ebullition constituted 0 to 84 ± 23% of the total fluxes with an average of 36 ± 24% throughout the entire study period (Table S3). The large uncertainty in the ratio of steady ebullition to total fluxes was mainly due to the uncertainty in total CH_4 fluxes (see Text S2 in the supporting information). To our knowledge, this is the first attempt to quantify steady ebullition fluxes from peat. However, the definitions of steady and episodic ebullition may depend on the detection sensitivity of measurement systems. Assuming that the mixing ratio of CH_4 to the total gases in a bubble is 0.2 [*Tokida et al*., 2007], the lowest observed ebullitive CH_4 release, 0.01 mg CH_4, suggests that a released gas bubble with volume lower than ~0.08 cm^3 may be classified as steady ebullition under the typical incubation conditions in this experiment. Following the exponentially decreasing trend in the lower end of the frequency distribution of ebullitive CH_4 releases (Figure 7), it is possible that the frequency of ebullitive CH_4 releases below 0.1 mg CH_4 would be much higher if the steady ebullition could be resolved by measurement systems of higher sensitivity.

We argue that the DFC implemented in a long-term chamber closure is a potentially superior technique to other more conventional methods for continuous CH_4 ebullition monitoring in peat. In many cases, the underlying mechanical processes in the peat matrix may be independent of the respective ambient or chamber CH_4 concentrations, plant physiology, and turbulence conditions of the chamber headspace [*Mastepanov and Christensen*, 2009]. Furthermore, all CH_4 exchange from the isolated monolith can be directly measured by DFC for months without missing any ebullition events. Given the high temporal resolution of the DFC, individual ebullition events can be explicitly identified even on a shorter time scale. Although the resolved pattern of CH_4 emission from the peat monolith may not be representative of other near-surface peat with different ecohydrological properties, in combination with additional constraints on C_{in} and diffusion and plant-mediated emissions, the DFC system has the potential to precisely partition pathways of CH_4 emissions in northern peatlands.

4.2. Couplings Between CH_4 Ebullition and Subsurface CH_4 Dynamics

Previous laboratory studies have found that even under careful wetting procedures, initial undersaturation occurred in undisturbed peat samples, such that the initial gas content ranged from 0.01 to 0.13 $m^3\ m^{-3}$ [*Baird et al*., 2004; *Strack et al*., 2005]. In our study, initial gas contents ranged from 0.04 to 0.07 $m^3\ m^{-3}$ for the three layers, and fast rates of gas buildup were observed before the first ebullition in week 2, especially for the middle and lower layers (Figure 5a). Although the time to the initiation of ebullition (10 days) was shorter than that measured in other studies [e.g., *Baird et al*., 2004] due possibly to the higher incubation temperature of this study, the gas contents at the first ebullition, 0.05 to 0.11 $m^3\ m^{-3}$, and maximum gas contents, 0.07 to 0.15 $m^3\ m^{-3}$, are consistent with the range reported in previous studies [*Baird et al*., 2004; *Strack et al*., 2005; *Kellner et al*., 2006]. We also found that the dissolved CH_4 concentrations in pore water during gas buildup and initial ebullition were below the theoretical equilibrium concentration (~8 mg L^{-1} [*Baird et al*., 2004]) previously assumed necessary for bubble formation (Figure 5b). Recently, *Laing et al*. [2008], using membrane inlet quadrupole mass spectrometry, found an average dissolved CH_4 concentration of 1.3 mg $CH_4\ L^{-1}$ to be equilibrated with gas bubbles comprising 11% by volume in shallow peat samples. Together with others, our findings support the argument that peatland CH_4 models only using nucleation to predict gas buildup and

ebullition likely need revision, because minute gas bubbles are always present in the peat pore space, causing a lowered equilibrium concentration for the dissolved phase and serving as initial nuclei for biogenic bubble growth [*Baird et al*., 2004; *Strack et al*., 2005].

Large reductions in dissolved CH_4 concentrations can occur during short time periods of active ebullition [*Strack and Waddington*, 2008]. In this study dissolved CH_4 concentrations correlated positively and significantly to gas contents in the upper layer ($R^2 = 0.65$, $P < 0.01$), but no significant correlation was detected in the middle and lower layers where gas contents were consistently larger ($P > 0.05$). Dissolved CH_4 concentrations resolved limited variations in episodic ebullition fluxes and frequency (Figures 6c and 6d). Due to its low solubility, CH_4 is predominantly stored in gaseous form even when a small bubble volume is present in the peat [*Strack and Waddington*, 2008]. The dominance of gaseous CH_4 in subsurface CH_4 stocks implies that dissolved CH_4 concentrations may be regulated by the storage and release of gas bubbles, resulting in dramatic changes in concentration during the main period of ebullition (Figure 5b). Another possibility is that CH_4 bubbles can be produced directly by granular microbial consortia containing methanogens such that dissolved CH_4 concentration is controlled by bubbles going into solution [*Green and Baird*, 2012]. Based on our observations, we suggest that gas bubble dynamics in near-surface peat may be decoupled from the dissolved CH_4 pool to a large extent and the physical characteristics of peat can then be important in determining ebullition fluxes [*Laing et al*., 2008].

As first proposed by *Baird et al*. [2004], peat soils may need to exceed a threshold bubble volume before ebullition can occur. In an effort to model ebullition based on this threshold theory, *Kellner et al*. [2006] further suggested that, rather than a single threshold value, a fuzzy threshold related to intrinsic properties of peat-bubble interactions is responsible for the complex ebullition behavior of peat. Despite its conceptual simplicity [*Coulthard et al*., 2009], the threshold theory has proven to be effective in several laboratory [*Comas and Slater*, 2007; *Slater et al*., 2007] and field [*Strack et al*., 2005] studies with resolved threshold gas content ranging from 0.07 to 0.16 $m^3\ m^{-3}$ for poorly decomposed near-surface *Sphagnum* peat. In our study, distinct differences in gas content and rate of gas bubble buildup among three layers were resolved (Figure 5a). While all three layers showed a significant linear relationship between gas content and ebullition fluxes, ebullition fluxes increased dramatically after the gas content of middle and lower layers leveled off at 0.14 (Figure 5a), an observation consistent with threshold-based ebullition. Thus, our work supports threshold theory using directly measured episodic CH_4 ebullition fluxes. More importantly, different relationships between gas content and episodic ebullition fluxes found in the three layers highlight that vertical heterogeneity of peat structure, an intrinsic property of peat commonly observed in northern peatlands [*Limpens et al*., 2008; *Comas et al*., 2013], may play a key role in controlling gas bubble dynamics even in this very shallow peat monolith.

The physical properties of peat, including the porosity, bulk density, decomposition degree, pore size distribution, and compressibility, exert a strong control on peatland ecohydrology and biogeochemistry [*Price et al*., 2005]. By using X-ray computed tomography, *Kettridge and Binley* [2011] concluded that the compressibility and the ability of *Sphagnum* peat to trap biogenic gas bubbles depend not only on the bulk volume of the peat constituents, which is usually inferred from the bulk density and porosity, but also on their spatial arrangement within the peat. The presence of longer structural components, like stems and branches, strongly increases the tortuosity of pore networks and the ability of peat to trap bubbles. In a laboratory study using electrical resistivity, *Slater et al*. [2007] revealed that biogenic gas bubbles tend to accumulate at certain depths (within 0.04 to 0.10 m below the water table in their case) within the shallow *Sphagnum* peat as thin layers due to the prevalently layered nature of peat. Based on such findings, differences in gas content and the relationship between gas content and episodic ebullition fluxes among three layers in our peat monolith may be attributed to layered structural differences in peat. The compressibility of peat decreases with increasing decomposition degree, and decomposed plant remnants can form a rigid framework in deep peat layers [*Price et al*., 2005]. In this study, more decomposed middle and lower layers with the presence of rigid root fibers and wood inclusions had higher bulk densities than the upper layer and may have denser and more tortuous pore networks to entrap gas bubbles [*Kettridge and Binley*, 2011]. The limited vertical deformation of the peat monolith might also be attributable to the layered formation of rigid structural components in the middle and lower layers. On the other hand, decreased compaction near the peat surface, together with the absence of rigid structural components, may make the upper layer less resistant to bubble release [*Comas and Slater*, 2007].

Interestingly, ebullition frequency increased linearly with gas content and did not exhibit a threshold effect (Figure 6b). While the upper layer with a lower bubble trapping potential might have a fast "bubble turnover" and be the source of small episodic ebullition events dominant in the ebullition frequency, large gas bubbles might be episodically vented from the middle and lower layers once the high ebullition threshold is reached. Therefore, we caution that the latest peatland CH_4 models applying a single ebullition threshold for the entire depth of peat [e.g., *Zhang et al*., 2012] may not be able to resolve the complex spatiotemporal pattern of CH_4 ebullition. Similarly, models adopting the pressure balance criteria to predict ebullition [e.g., *Tang et al*., 2010] may not be able to capture large ebullition events originating from deep peat layers where the bubble trapping potential is much higher and overpressurized strata are formed. We propose that a depth-dependent multithreshold model determined by peat physical structure should be adopted in CH_4 models as the criteria for ebullition prediction.

4.3. Relative Importance of Atmospheric Pressure and Temperature as Ebullition Trigger

Both atmospheric pressure and temperature have been identified as ebullition triggers (Table 1). Optimal temperatures for CH_4 production have been found to be between 10°C and 12°C for northern peat samples [*Williams and Crawford*, 1984]. *Bergman et al*. [1998] suggested that high-temperature incubations (above 20°C in their case) of *Sphagnum* peat tend to decouple CH_4 production from temperature. In this sense, a temperature higher than the optimal range for CH_4 production is desirable to minimize its biological control on CH_4 ebullition. On the other hand, an approximately 4°C fluctuation in the diel cycle (Figure 3), theoretically identical to a 40 hPa change in atmospheric pressure in terms of driving bubble volume alteration [*Tokida et al*., 2009], is sufficiently large to assess the triggering effects of temperature changes.

In week 2 to week 5, ebullitive CH_4 releases had no significant difference between daytime and nighttime (Figure 8a), and ebullition fluxes had weak relationship with changes in atmospheric pressure (Figure 8c), indicating that both changes in temperature and atmospheric pressure had limited controls on CH_4 ebullition when gas contents were far below the ebullition thresholds. When the bubble buildup in the middle and lower layers was substantial in week 6 to week 8, the ebullition frequency increased greatly in the daytime (Figure 8b). If the increased daytime temperature was able to trigger large episodic ebullition from the middle and lower layers during this time period, we would expect to see outliers of ebullitive CH_4 releases, illustrated by the length of upper error bars for every experimental hour in Figure 8b, during daytime. In fact, however, those outliers tended to occur at nighttime (Figure 8b) and were often found to be coupled with large drops in atmospheric pressure, leading to substantial increases in time-integrative ebullitive CH_4 releases (Figure 8d). Therefore, the negative linear relationship between cumulative ebullitive CH_4 releases and changes in atmospheric pressure (most significant between weeks 6 and 8) (Figure 8d) further suggests that atmospheric pressure was responsible for triggering larger CH_4 ebullition from deeper layers where big bubbles were trapped.

Previous studies have illustrated that the thermal conductivity of peat decreases with water content and decomposition degree [*Yoshikawa et al*., 2003]. In our study, the unsaturated moss layer in the upper 2 cm might insulate the deeper layers from warm air in the daytime. In addition, even below the water table, poorly decomposed surface peat of low thermal conductivity might also dampen the amplitude of downward heat flux to some extent [*van der Molen and Wijmstra*, 1994; *Yoshikawa et al*., 2003; *O'Donnell et al*., 2009]. Although we do not have enough information on the temperature dynamics of deeper layers, as implied by other studies [e.g., *Tokida et al*., 2007], the diel temperature cycle in the middle and lower layers might be small. Therefore, we speculated that the triggering effects of temperature were mostly limited to the upper layer where a low ebullition threshold existed, which resulted in small and frequent ebullitive CH_4 releases (Figure 8b) constituting the majority of the total episodic ebullition flux integrated over the entire experiment (Figure 7). On the other hand, atmospheric pressure is related directly to pressure of gas bubbles below the water table, such that changes in atmospheric pressure may have stronger triggering effects on bubbles trapped in deep peat layers. The resultant large ebullitive releases, while making only a limited contribution to the total episodic ebullition on monthly scale (Figure 7), may dominate short-term CH_4 fluxes during time periods of falling atmospheric pressure (Figure 8d). While increasing atmospheric pressure may facilitate small ebullition events from upper layers of the peat by allowing compressed gas bubbles to pass through fiber networks [*Comas and Wright*, 2012], the results from this near-surface peat monolith suggest that large buoyancy controlled ebullition events originating from deeper layers are most likely triggered by drops in

atmospheric pressure. Despite the fact that the observed triggering effects of atmospheric pressure and temperature are specific to the peat monolith studied, the outlined couplings between the peat physical structure and changes in atmospheric pressure and temperature as ebullition triggers are very likely to be applicable in other cases and suffice for setting the stage for future investigation and modeling.

5. Conclusions

In this study, we successfully demonstrated the capability of DFC for continuously monitoring CH_4 ebullition from a near-surface *Sphagnum* peat and its potential to partition the pathways of CH_4 emission. The application of DFC with coupled subsurface gas content and dissolved CH_4 concentration measurements at the laboratory scale offers new opportunities for understanding the complex behavior of CH_4 ebullition and its couplings to subsurface gas bubble dynamics. Our work highlights a need to integrate peat physical structure into ebullition models. The structural heterogeneity of peat gives rise to a depth-dependent multithreshold model that was responsible for the spatiotemporal variation of CH_4 ebullition and partially determines the relative importance of changes in atmospheric pressure and temperature in triggering ebullitive CH_4 releases. Although this work relied on just one peat monolith, the outlined mechanisms behind CH_4 ebullition in peat may be of broad significance to other studies of near-surface peat in boreal settings. Future efforts will be dedicated to applying the DFC technique at the field scale to better improve our knowledge of CH_4 ebullition in northern peatlands.

Acknowledgments
This material is based upon work supported by the National Science Foundation under grant EAR-1045084. The authors thank Neil Terry (Rutgers-Newark) for his help during the field sampling.

References

Baird, A., C. W. Beckwith, S. Waldron, and J. M. Waddington (2004), Ebullition of methane-containing gas bubbles from near-surface *Sphagnum* peat, *Geophys. Res. Lett.*, *31*, L21505, doi:10.1029/2004GL021157.

Beckmann, M., S. K. Sheppard, and D. Lloyd (2004), Mass spectrometric monitoring of gas dynamics in peat monoliths: Effects of temperature and diurnal cycles on emissions, *Atmos. Environ.*, *38*, 6907–6913, doi:10.1016/j.atmosenv.2004.08.004.

Bergman, I., B. H. Svensson, and M. Nilsson (1998), Regulation of methane production in a Swedish acid mire by pH, temperature and substrate, *Soil Biol. Biochem.*, *30*(6), 729–741, doi:10.1016/S0038-0717(97)00181-8.

Bragazza, L., J. Parisod, A. Buttler, and R. D. Bardgett (2012), Biogeochemical plant-soil microbe feedback in response to climate warming in peatlands, *Nat. Clim. Change*, *3*(3), 273–277, doi:10.1038/nclimate1781.

Bridgham, S. D., H. Cadillo-Quiroz, J. K. Keller, and Q. Zhuang (2013), Methane emissions from wetlands: Biogeochemical, microbial, and modeling perspectives from local to global scales, *Global Change Biol.*, *19*, 1325–1346, doi:10.1111/gcb.12131.

Christensen, T. R., N. Panikov, M. Mastepanov, A. Joabsson, A. Stewart, M. Öquist, M. Sommerkorn, S. Reynaud, and B. Svensson (2003), Biotic controls on CO_2 and CH_4 exchange in wetlands—A closed environment study, *Biogeochemistry*, *64*, 337–354, doi:10.1023/A:1024913730848.

Comas, X., and L. Slater (2007), Evolution of biogenic gases in peat blocks inferred from noninvasive dielectric permittivity measurements, *Water Resour. Res.*, *43*, W05424, doi:10.1029/2006WR005562.

Comas, X., and W. Wright (2012), Heterogeneity of biogenic gas ebullition in subtropical peat soils is revealed using time-lapse cameras, *Water Resour. Res.*, *48*, W04601, doi:10.1029/2011WR011654.

Comas, X., L. Slater, and A. Reeve (2008), Seasonal geophysical monitoring of biogenic gases in a northern peatland: Implications for temporal and spatial variability in free phase gas production rates, *J. Geophys. Res.*, *113*, G01012, doi:10.1029/2007JG000575.

Comas, X., N. Kettridge, A. Binley, L. Slater, A. Parsekian, A. J. Baird, and J. M. Waddington (2013), The effect of peat structure on the spatial distribution of biogenic gases within bogs, *Hydrol. Process.*, doi:10.1002/hyp.10056.

Coulthard, T. J., A. J. Baird, J. Ramirez, and J. M. Waddington (2009), Methane dynamics in peat: Importance of shallow peats and a novel reduced-complexity approach for modeling ebullition, in *Northern Peatlands and Carbon Cycling*, edited by A. Baird et al., pp. 173–185, AGU, Washington, D. C.

Dingman, S. L. (1994), *Physical Hydrology*, Prentice Hall, Upper Saddle River, N. J.

Fechner-Levy, E. J., and H. F. Hemond (1996), Trapped methane volume and potential effects on methane ebullition in a northern peatland, *Limnol. Oceanogr.*, *41*(7), 1375–1383, doi:10.4319/lo.1996.41.7.1375.

Gao, F., and S. R. Yates (1998), Laboratory study of closed and dynamic flux chambers: Experimental results and implications for field application, *J. Geophys. Res.*, *103*(D20), 26,115–26,125, doi:10.1029/98JD01346.

Glaser, P. H., J. P. Chanton, P. Morin, D. O. Rosenberry, D. I. Siegel, O. Ruud, L. I. Chasar, and A. S. Reeve (2004), Surface deformations as indicators of deep ebullition fluxes in a large northern peatland, *Global Biogeochem. Cycles*, *18*, GB1003, doi:10.1029/2003GB002069.

Goodrich, J. P., R. K. Varner, S. Frolking, B. N. Duncan, and P. M. Crill (2011), High-frequency measurements of methane ebullition over a growing season at a temperate peatland site, *Geophys. Res. Lett.*, *38*, L07404, doi:10.1029/2011GL046915.

Green, S. M., and A. J. Baird (2012), A mesocosm study of the role of the sedge *Eriophorum angustifolium* in the efflux of methane—including that due to episodic ebullition—from peatlands, *Plant Soil*, *351*, 207–218, doi:10.1007/s11104-011-0945-1.

Green, S. M., and A. J. Baird (2013), The importance of episodic ebullition methane losses from three peatland microhabitats: A controlled-environment study, *Eur. J. Soil Sci.*, *64*, 27–36, doi:10.1111/ejss.12015.

Hutchinson, G. L., G. P. Livingston, R. W. Healy, and R. G. Striegl (2000), Chamber measurement of surface-atmosphere trace gas exchange: Numerical evaluation of dependence on soil, interfacial layer, and source/sink properties, *J. Geophys. Res.*, *105*(D7), 8865–8875, doi:10.1029/1999JD901204.

Kellner, E., J. M. Waddington, and J. S. Price (2005), Dynamics of biogenic gas bubbles in peat: Potential effects on water storage and peat deformation, *Water Resour. Res.*, *41*, W08417, doi:10.1029/2004WR003732.

Kellner, E., A. J. Baird, M. Oosterwoud, K. Harrison, and J. M. Waddington (2006), Effect of temperature and atmospheric pressure on methane (CH_4) ebullition from near-surface peats, *Geophys. Res. Lett.*, *33*, L18405, doi:10.1029/2006GL027509.

Kettridge, N., and A. Binley (2011), Characterization of peat structure using X-ray computed tomography and its control on the ebullition of biogenic gas bubbles, *J. Geophys. Res.*, *116*, G01024, doi:10.1029/2010JG001478.

Lai, D. Y. F., N. T. Roulet, E. R. Humphreys, T. R. Moore, and M. Dalva (2012), The effect of atmospheric turbulence and chamber deployment period on autochamber CO_2 and CH_4 flux measurements in an ombrotrophic peatland, *Biogeosciences*, *9*, 3305–3322, doi:10.5194/bg-9-3305-2012.

Laing, C. G., T. G. Shreeve, and D. M. E. Pearce (2008), Methane bubbles in surface peat cores: *In situ* measurements, *Global Change Biol.*, *14*, 916–924, doi:10.1111/j.1365-2486.2007.01534.x.

Limpens, J., F. Berendse, C. Blodau, J. G. Canadell, C. Freeman, J. Holden, N. Roulet, H. Rydin, and G. Schaepman-Strub (2008), Peatlands and the carbon cycle: From local processes to global implications—A synthesis, *Biogeosciences*, *5*(5), 1475–1491, doi:10.5194/bg-5-1475-2008.

Mastepanov, M., and T. R. Christensen (2009), Laboratory investigations of methane buildup in, and release from, shallow peats, in *Northern Peatlands and Carbon Cycling*, edited by A. Baird et al., pp. 205–218, AGU, Washington D. C.

McDermitt, D., et al. (2011), A new low-power, open-path instrument for measuring methane flux by eddy covariance, *Appl. Phys. B*, *102*, 391–405, doi:10.1007/s00340-010-4307-0.

Nielson, K. K., V. C. Rogers, and G. W. Gee (1984), Diffusion of radon through soils: A pore distribution model, *Soil Sci. Soc. Am. J.*, *48*(3), 482–487, doi:10.2136/sssaj1984.03615995004800030002x.

O'Donnell, J. A., V. E. Romanovsky, J. W. Harden, and A. D. McGuire (2009), The effect of moisture content on the thermal conductivity of moss and organic soil horizons from black spruce ecosystems in interior Alaska, *Soil Sci.*, *174*(12), 646–651, doi:10.1097/SS.0b013e3181c4a7f8.

Panikov, N. S., M. A. Mastepanov, and T. R. Christensen (2007), Membrane probe array: Technique development and observation of CO_2 and CH_4 diurnal oscillations in peat profile, *Soil Biol. Biochem.*, *39*(7), 1712–1723, doi:10.1016/j.soilbio.2007.01.034.

Pape, L., C. Ammann, A. Nyfeler-Brunner, C. Spirig, K. Hens, and F. X. Meixner (2009), An automated dynamic chamber system for surface exchange measurement of non-reactive and reactive trace gases of grassland ecosystems, *Biogeosciences*, *6*, 405–429, doi:10.5194/bg-6-405-2009.

Parsekian, A. D., L. Slater, and D. Giménez (2012), Application of ground-penetrating radar to measure near-saturation soil water content in peat soils, *Water Resour. Res.*, *48*, W02533, doi:10.1029/2011WR011303.

Price, J. S., J. Cagampan, and E. Kellner (2005), Assessment of peat compressibility: Is there an easy way?, *Hydrol. Process.*, *19*(17), 3469–3475, doi:10.1002/hyp.6068.

Reid, M. C., R. Tripathee, K. V. R. Schäfer, and P. R. Jaffé (2013), Tidal march methane dynamics: Difference in seasonal lags in emissions driven by storage in vegetated versus unvegetated sediments, *J. Geophys. Res. Biogeosci.*, *118*, 1802–1813, doi:10.1002/jgrg.20152.

Rosenberry, D. O., P. H. Glaser, D. I. Siegel, and E. P. Weeks (2003), Use of hydraulic head to estimate volumetric gas content and ebullition flux in northern peatlands, *Water Resour. Res.*, *39*(3), 1066, doi:10.1029/2002WR001377.

Rothfuss, F., and R. Conrad (1998), Effect of gas bubbles on the diffusive flux of methane in anoxic paddy soil, *Limnol. Oceanogr.*, *43*(7), 1511–1518, doi:10.4319/lo.1998.43.7.1511.

Slater, L. D., and A. Reeve (2002), Investigating peatland stratigraphy and hydrogeology using integrated electrical geophysics, *Geophysics*, *67*(2), 365–378, doi:10.1190/1.1468597.

Slater, L., X. Comas, D. Ntarlagiannis, and M. R. Moulik (2007), Resistivity-based monitoring of biogenic gases in peat soils, *Water Resour. Res.*, *43*, W10430, doi:10.1029/2007WR006090.

Stamp, I., A. J. Baird, and C. M. Heppell (2013), The importance of ebullition as a mechanism of methane (CH_4) loss to the atmosphere in a northern peatland, *Geophys. Res. Lett.*, *40*, 1–4, doi:10.1002/grl.50501.

Stephen, K. D., J. R. M. Arah, K. L. Thomas, J. Benstead, and D. Lloyd (1998), Gas diffusion coefficient profile in peat determined by modelling mass spectrometric data: Implications for gas phase distribution, *Soil Biol. Biochem.*, *30*(3), 429–431, doi:10.1016/S0038-0717(97)00118-1.

Strack, M., E. Kellner, and J. M. Waddington (2005), Dynamics of biogenic gas bubbles in peat and their effects on peatland biogeochemistry, *Global Biogeochem. Cycles*, *19*, GB1003, doi:10.1029/2004GB002330.

Strack, M., and J. M. Waddington (2008), Spatiotemporal variability in peatland subsurface methane dynamics, *J. Geophys. Res.*, *113*, G02010, doi:10.1029/2007JG000472.

Tang, J., Q. Zhuang, R. D. Shannon, and J. R. White (2010), Quantifying wetland methane emissions with process-based models of different complexities, *Biogeosciences*, *7*(4), 6121–6171, doi:10.5194/bgd-7-6121-2010.

Taylor, J. (1997), *An Introduction to Error Analysis: The Study of Uncertainties in Physical Measurements*, 2nd ed., Univ. Sci., Sausalito, Calif.

Tokida, T., T. Miyazaki, and M. Mizoguchi (2005), Ebullition of methane from peat with falling atmospheric pressure, *Geophys. Res. Lett.*, *32*, L13823, doi:10.1029/2005GL022949.

Tokida, T., T. Miyazaki, M. Mizoguchi, O. Nagata, F. Takakai, and A. Kagemoto (2007), Falling atmospheric pressure as a trigger for methane ebullition from peatland, *Global Biogeochem. Cycles*, *21*, GB2003, doi:10.1029/2006GB002790.

Tokida, T., T. Miyazaki, and M. Mizoguchi (2009), Physical controls on ebullition losses of methane from peatlands, in *Northern Peatlands and Carbon Cycling*, edited by A. Baird et al., pp. 219–228, AGU, Washington, D. C.

Treat, C. C., J. L. Bubier, R. K. Varner, and P. M. Crill (2007), Timescale dependence of environmental and plant-mediated controls on CH_4 flux in a temperate fen, *J. Geophys. Res.*, *112*, G01014, doi:10.1029/2006JG000210.

Turetsky, M. R., C. C. Treat, M. P. Waldrop, J. M. Waddington, J. W. Harden, and A. D. McGuire (2008), Short-term response of methane fluxes and methanogen activity to water table and soil warming manipulations in an Alaskan peatland, *J. Geophys. Res.*, *113*, G00A10, doi:10.1029/2007JG000496.

van der Molen, P. C., and T. A. Wijmstra (1994), The thermal regime of hummock-hollow complexes on Clara bog, Co. Offaly, *Proc. R. Irish Acad. B*, *94*, 209–221.

Waddington, J. M., K. Harrison, E. Kellner, and A. J. Baird (2009), Effect of atmospheric pressure and temperature on entrapped gas content in peat, *Hydrol. Process.*, *23*, 2970–2980, doi:10.1002/hyp.7412.

Webb, E. K., G. I. Pearman, and R. Leuning (1980), Correction of flux measurements for density effects due to heat and water vapour transfer, *Q. J. R. Meteorolog. Soc.*, *106*, 85–100, doi:10.1002/qj.49710644707.

Wiesenburg, D. A., and N. L. Guinasso Jr. (1979), Equilibrium solubilities of methane, carbon monoxide, and hydrogen in water and sea water, *J. Chem. Eng. Data*, *24*(4), 356–360, doi:10.1021/je60083a006.

Williams, R. T., and R. L. Crawford (1984), Methane production in Minnesota peatlands, *Appl. Environ. Microbiol.*, *46*(6), 1266–1271.

Wuebbles, D. J., and K. Hayhoe (2002), Atmospheric methane and global change, *Earth Sci. Rev.*, *57*(3), 177–210, doi:10.1016/S0012-8252(01)00062-9.

Yoshikawa, K., W. R. Bolton, V. E. Romanovshy, M. Fukuda, and L. D. Hinzman (2003), Impacts of wildfire on the permafrost in the boreal forests of Interior Alaska, *J. Geophys. Res.*, *108*(D1), 8148, doi:10.1029/2001JD000438.

Zhang, Y., T. Sachs, C. Li, and J. Boike (2012), Upscaling methane fluxes from closed chambers to eddy covariance based on a permafrost biogeochemistry integrated model, *Global Change Biol.*, *18*, 1428–1440, doi:10.1111/j.1365-2486.2011.02587.x.